J Mol Model (2012) 18:4819–4830
DOI 10.1007/s00894-012-1486-0

ORIGINAL PAPER

Computational investigation of the adsorption of carbon dioxide onto zirconium oxide clusters

Pascal Boulet · Christina Knöfel · Bogdan Kuchta · Virginie Hornebecq · Philip L. Llewellyn

Received: 22 December 2011 / Accepted: 28 May 2012 / Published online: 16 June 2012

Abstract A theoretical investigation of the adsorption of CO_2 onto ZrO_2 is presented. Various cluster models were used to mimic different basic and acidic sites on the surface. The method used was the density functional theory with the generalized gradient approximation and including Grimme's empirical model in order to properly describe the weak interactions that may occur between the adsorbate and the surface. We found that the adsorption at sites exhibiting two adjacent unsaturated zirconium atoms led to either the exothermic dissociation of CO_2 or to a strongly physisorbed state. By contrast, on a single unsaturated zirconium, CO_2 was adsorbed in an apical manner. In this case, the molecule is highly polarized and the adsorption energy amounts to −64.6 kJ mol^{-1}. Finally, the weakest adsorption of CO_2 occurred on the basic OH sites on the surface.

Keywords Carbon dioxide · Zirconium oxide · Clusters · Computational chemistry · Density functional theory

Introduction

For the last three decades, zirconium dioxide has found an increasingly wide range of applications due to its interesting properties as a ceramic material. Properties such as its high temperature resistance (its melting point is around 3000 K) and corrosion resistance, as well as its combination of acidic, basic, oxidizing, and reducing properties [1], have prompted its use in a large number of applications, such as thin-film coating [2] and catalysis [3–10]. The chemisorption of CO_2 has been intensively studied from an experimental viewpoint, particularly using infrared spectroscopy [11–16]. By contrast, as far as we know, theoretical investigations of the adsorption of CO_2 onto ZrO_2 are rare [17], or even totally absent if we focus on theoretical insights obtained from density functional theory calculations.

The aim of the work described in this paper was to study the adsorption of CO_2 onto various clusters of ZrO_2 at the density functional theory level. Details about the theoretical approach used are presented in the next section, followed by a description of the results. The third part of this paper describes a comparative analysis of the adsorption of CO_2 onto various oxide supports.

P. Boulet (✉) · C. Knöfel · B. Kuchta · V. Hornebecq · P. L. Llewellyn
Laboratoire Matériaux Divisés Interfaces Réactivité Electrochimie, UMR 7246, Aix-Marseille Université et CNRS, Avenue de l'Escadrille Normandie-Niemen, 13397 Marseille Cedex, France
e-mail: pascal.boulet@univ-provence.fr

Present Address:
C. Knöfel
Risø National Laboratory for Sustainable Energy, Fuel Cells and Solid State Chemistry Division, ABF, P.O. Box 49, Frederiksborgvej 399, DK-4000 Roskilde, Denmark

Theoretical approach

In this section we describe the computational strategy that we used and the model clusters of ZrO_2 that were designed in order to study the adsorption of the molecule.

Theory

The calculations were performed with the meta-GGA (generalized gradient approximation) TPSS exchange-correlation functional [18]. This ab initio functional, which is based on the PKZB one [19] and contains the PBE [20] GGA functional, improves upon the physical descriptions of systems provided by these two functionals by requiring that the meta-

GGA exchange potential is finite at the nucleus for ground-state one- and two-electron densities [18]. Indeed, when PBE fails, TPSS improves the description of the property of interest (see, for instance, [21–24]). In addition, because the system contains CO_2 as the adsorbate species, we accounted for the dispersion interactions by using Grimme's approach, which consists of inserting an empirical C_6/r^6 potential into the Hamiltonian (see [25] and references therein).

The all-electron TZVP basis set of localized atomic orbitals developed by Ahlrichs et al. [26] was used to optimize the geometrical parameters of the structures. The BSSE (basis set superposition error) was corrected for using the Boys and Bernardi approach [27]. In addition, for sake of comparison, the TZV(2df,2pd)++ basis set was utilized to obtain the total energies in conjugation with the TZVP-optimized structures. Later, we will see that a sizeable effect on the adsorption energies is observable. However, because pseudopotentials were not available, it was not possible to optimize the structures with such a large basis set. In addition, since we were most interested in observing the trends in both the adsorption energies and the intermolecular interactions, not in obtaining accurate absolute adsorption energies, we believe that our approach was sufficient for our purpose.

In order to speed up the calculations, the resolution of the identity algorithm was used [28–34]. The ORCA 2.6.35 software package was used throughout [35].

Structure of the clusters

At room temperature, zirconium oxide crystallizes into a monoclinic structure (group 14, P21/c) known as baddeleyite [36]. Phase transformations occur at high temperatures, leading to tetragonal structures near 1440 K [37, 38] and the cubic one of the fluorite type (group 225, Fm-3 m) near to 2370 K [39].

The clusters used in this work were built from the cubic form of zirconia. The dangling bonds were saturated with hydrogen atoms. The positions of these atoms were optimized while the remaining atoms were kept fixed at their crystallographic positions. Two types of sites were considered in this study: those that exhibit naked zirconium atoms at the surface (to model reduced active sites) and those that are oxidized by either oxygen atoms or hydroxyl groups that interact with the adsorbate. We only considered uncharged adsorption sites in this work.

The smallest cluster used to model the adsorption of CO_2 contained only two zirconium atoms, leading to the stoichiometry $Zr_2O_{14}H_{20}$. The corresponding structure is depicted in Fig. 1a. This cluster contains an oxygen atom bridging the two zirconium atoms. Two clusters containing three zirconium atoms, as shown in Fig. 1b and c, had stoichiometries of $Zr_3O_{16}H_{20}$ and $Zr_3O_{19}H_{26}$. The first cluster allowed us to model the adsorption onto a capping oxygen, and corresponds to the (111) basal plane. The $Zr_3O_{19}H_{26}$ cluster was almost identical to the previous one except that it represented an oxidized adsorption site with surface hydroxyl groups. $Zr_4O_{16}H_{16}$, which bears four Zr atoms (Fig. 1d), allowed us to model adsorption on the (001) basal plane. Here, two out of the four Zr atoms were available for interactions with a CO_2 molecule. Hence, it corresponded to a strongly reduced adsorption site. Finally, $Zr_5O_{24}H_{28}$, which was the largest cluster used (Fig. 1e), contains one accessible Zr atom on the surface. It was used to model the (001) basal plane.

Results

The results for the structural parameters and atomic charge of CO_2 calculated at the TPSS/TZVP//TZV(2df,2dp)++ level are given in Table 1. The C–O bond length is 117 pm, which is only 3.5 % larger than the experimentally measured length (113.1 pm), as obtained from microwave spectroscopy [40].

The total energies of the structures and the adsorption energies of CO_2 on the various clusters are reported in Table 2. The adsorption energies calculated with at the BSSE-uncorrected level (TZVP basis set) are predicted to be greater than those calculated with the larger basis set TZV(2df,2pd)++, the exception being the case where CO_2 is adsorbed onto the $Zr_4O_{16}H_{16}$ cluster. The difference in adsorption energy amounts to about 5 kJ mol^{-1} for the small clusters containing two or three Zr atoms, but more than 20 kJ mol^{-1} for the largest cluster. We can see that the differences between the BSSE-corrected adsorption energies and those calculated with the TZV(2df,2dp)++ basis set are small for the small clusters (with less than four zirconium atoms). The mean average difference amounts to only 3 %. This contrasts with the case for the two largest clusters, which show much larger differences (9 % and 22 % for $Zr_4O_{16}H_{16}$ and $Zr_5O_{24}H_{28}$, respectively). In addition, the BSSE correction slightly increases (on average) with cluster size. This observation has already been reported by Fuentealba et al. in their study of the BSSE in copper clusters Cu_n ($1 \le n \le 13$) [41], although the authors claimed that these results may not be transferable to other systems.

The nondissociative adsorption energies vary from −25 kJ mol^{-1} to −65 kJ mol^{-1} (if one excludes the case of the $Zr_4O_{16}H_{16}$ cluster, for which the description is given in the next paragraph) depending on the type of cluster and the nature of the surface atoms that interact with CO_2. The weakest adsorption energies (−24.9 kJ mol^{-1} and −32.6 kJ mol^{-1}) correspond to adsorption onto a surface oxygen ($Zr_2O_{14}H_{20}$ and $Zr_3O_{16}H_{20}$). In both cases, CO_2 is adsorbed parallel to the surface: either CO_2 is aligned with the Zr–O–Zr axis (Fig. 2b) or it is slightly tilted with respect to this axis (25°, see Fig. 2a), in order to increase the interactions between the CO_2 oxygen and the surface hydroxyl groups. The adsorption distance ranges from 210 pm to 270 pm, depending on the structure

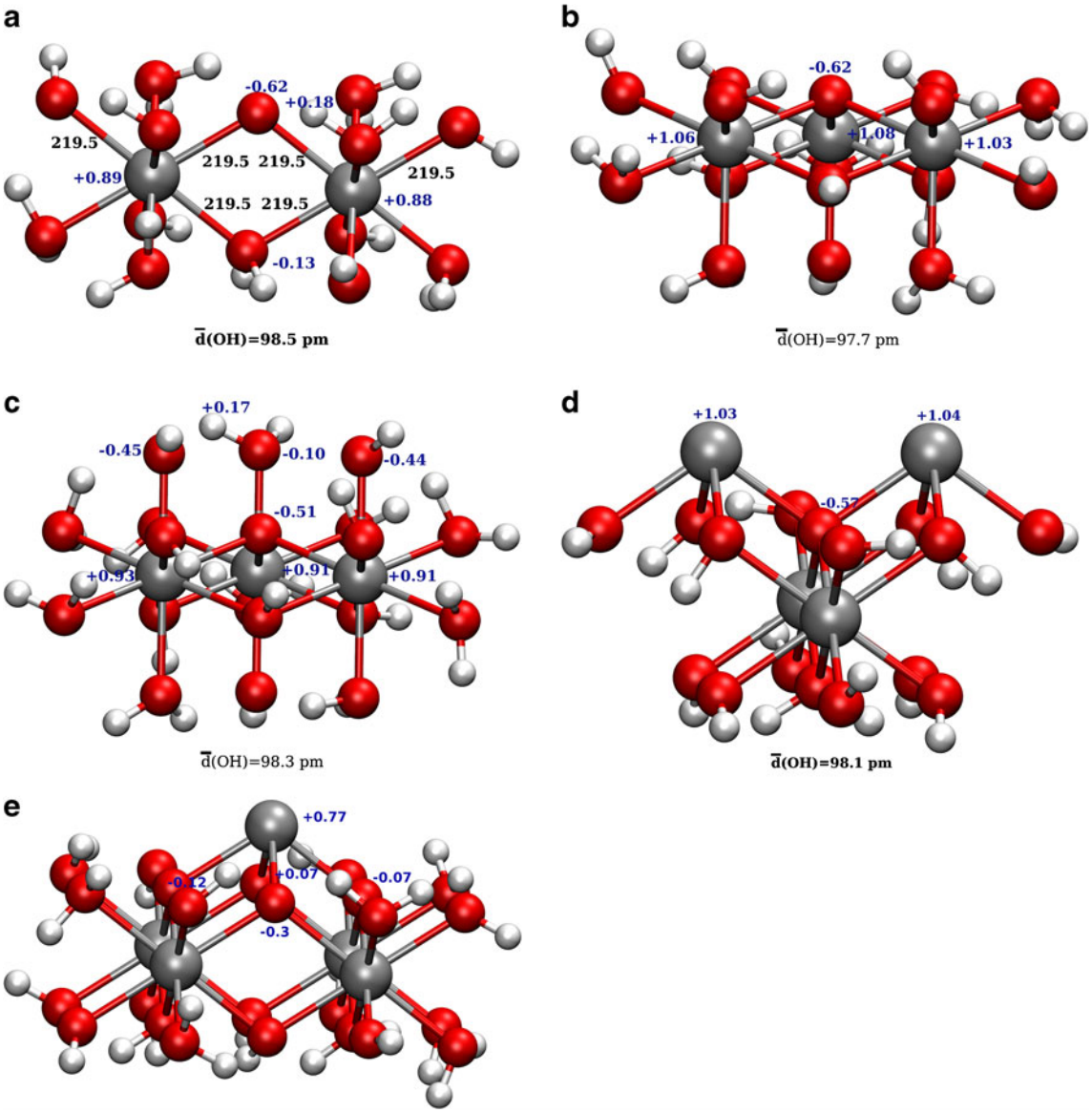

Fig. 1 Structures of the neutral clusters of zirconia used in this study. The bond distances Zr–O correspond to the crystallographic ones. The signed values correspond to the Mulliken charges. **a** $Zr_2O_{14}H_{20}$ with a bridging oxygen. **b** $Zr_3O_{16}H_{20}$ with a capping oxygen atom. **c** $Zr_3O_{19}H_{26}$ with hydroxyl groups. **d** $Zr_4O_{16}H_{16}$ exhibits two zirconium atoms that are available for interactions with CO_2. **e** $Zr_5O_{24}H_{28}$ is a reduced site with one Zr atom on the surface

considered. The Mulliken charges on the atoms of the clusters $Zr_2O_{14}H_{20}$ and $Zr_3O_{16}H_{20}$ (Fig. 1a and b) are barely modified when CO_2 is adsorbed (Fig. 2a and b). For the clusters, the charge on the central oxygen is −0.63 $|e|$, and those on the Zr atoms are around +1.0 $|e|$ (for $Zr_3O_{16}H_{20}$). The adsorbent therefore seems unperturbed by the adsorption of CO_2. By contrast, the charges on the adsorbate are significantly decreased (by a factor of 2) with respect to those on the free molecule. It appears that the adsorption process leads to a redistribution of the electron density inside the adsorbate. Analysis of the frontier orbitals shows that in the absence of CO_2, the HOMO (highest occupied molecular orbital) of $Zr_2O_{14}H_{20}$ (Fig. 3a) possesses π* character and is localized on the oxygen atoms, while the LUMO (lowest unoccupied molecular orbital) corresponds mainly to the d_{z2} orbital of Zr (Fig. 3b). For the cluster $Zr_3O_{16}H_{20}$, the HOMO again has π* character and is localized on the oxygen atoms, while the LUMO is more

Table 1 Structural and electronic data for CO_2 obtained at the TPSS/TZVP//TZV(2df,2dp)++ level of approximation

Property	Calculated data
C–O bond distance (pm)	117
O–C–O bond angle (°)	180
Mulliken charge (e)	q(O) = −0.2; q(C) = 0.4

Table 2 Total energies and adsorption energies calculated at the TPSS/TZVP and TPSS/TZVP//TZV(2df,2pd)++ levels of theory. For adsorption onto $Zr_4O_{16}H_{16}$, two types of adsorption state were found for CO_2: a physisorbed one termed $CO_2^{(ad)}$ and a dissociated one termed $CO_2^{(di)}$, where CO_2 gives (CO + O) adsorbed onto the cluster

Structures	Total energy (Ha) TZVP	Adsorption energy (kJ mol^{-1}) TZVP	Adsorption energy including the basis set superposition error (kJ mol^{-1})	Total energy (Ha) TZV(2df,2pd)++	Adsorption energy (kJ mol^{-1}) TZV(2df,2pd)++
CO_2	−188.684082	–	–	−188.695373	–
$Zr_2O_{14}H_{20}$	−8147.954923	–	–	−8148.042728	–
$CO_2/Zr_2O_{14}H_{20}$	−8336.653308	−37.5	−33.5	−8336.750504	−32.6
$Zr_3O_{16}H_{20}$	−11839.646423	–	–	−11839.751938	–
$CO_2/Zr_3O_{16}H_{20}$	−12028.341847	−29.8	−24.4	−12028.456800	−24.9
$Zr_3O_{19}H_{26}$	−12069.050891	–	–	−12069.173549	–
$CO_2/Zr_3O_{19}H_{26}$	−12257.750317	−40.3	−35.5	−12257.881848	−33.9
$Zr_4O_{16}H_{16}$	−15377.974895	–	–	−15378.077611	–
$CO_2^{(ad)}/Zr_4O_{16}H_{16}$	−15566.772927	−299.2	−289.1	−15566.896948	−325.5
$CO_2^{(di)}/Zr_4O_{16}H_{16}$	−15566.760640	−266.9	−261.4	−15566.880555	−282.4
$Zr_5O_{24}H_{28}$	−19528.776008	–	–	−19528.935740	–
$CO_2/Zr_5O_{24}H_{28}$	−19717.4492961	−86.3	−83.0	−19717.655722	−64.6

localized on the Zr atoms (d_{z2} and d_{xy} orbitals, Fig. 4a and b). These characteristics are clearly unmodified by the presence of CO_2 (Figs. 3c and d and 4c and d). However, we can see that the electron density on the clusters is slightly increased when CO_2 is present (all of the contour plot isovalues being equal for comparison). It is likely, then, that a small amount of the redistributed charge from CO_2 is transferred to the surface.

The adsorption of CO_2 onto oxidized surfaces is slightly more energetic. In the case of the cluster $Zr_3O_{19}H_{26}$, the adsorption energy amounts to −33.9 kJ mol^{-1}. The distance of the adsorbate from the substrate is large (260 pm), which explains the relatively weak interaction energy. The atomic charges on the naked cluster are only weakly modified by the presence of CO_2 (Figs. 1c and 2c). The same observations can be made about the frontier orbitals as before: the HOMO possesses π* character (surface oxygen atoms) and the LUMO corresponds to the Zr d_{z2} and d_{xy} orbitals, whether CO_2 is adsorbed onto the cluster or not (Fig. 5).

Two possible states were found for the adsorption of CO_2 onto the cluster $Zr_4O_{16}H_{16}$, which has two unsaturated zirconium atoms.

The first one is obtained with a starting structure where the Zr–O–Zr–O–C–O sequence of atoms forms a six-membered ring in which O–C–O is linear. Geometry minimization leads to the strong adsorption of CO_2 where the molecule is strongly bent (128.4°) and the carbon atom is capping both zirconium atoms. The atoms of Zr_2CO_2 are coplanar. The C–O bond lengths are drastically elongated (128.5 pm on average) compared to the gas-phase molecule (117.0 pm). The Zr–C bond distance is 238.8 pm on average, which is about 20 pm longer than the Zr–O bond in the ZrO_2 crystal. There is a net charge transfer from the surface, which bears a charge of +0.5 |*e*|, to the molecule (−0.5 |*e*|, *q*(C)=+0.22 |*e*|, *q*(O)=−0.36 |*e*|). Furthermore, the structure exhibits a strong dipole moment of 3.15 D. As a consequence, most of the interaction between the cluster and the molecule arises from electrostatic forces, which may explain the extremely strong adsorption energy of the CO_2 molecule onto $Zr_4O_{16}H_{16}$ (−325.5 kJ mol^{-1}).

The second adsorption state corresponds to the dissociation of the molecule into the adsorbed CO species and a remaining oxygen atom linking both zirconium atoms. This state is obtained when the CO_2 molecule approaches the cluster with an apical orientation, where one of the oxygen atoms of CO_2 is located equidistant from the Zr atoms. In this case, the dissociation process is spontaneous, and no reaction path with a local adsorption minimum and transition state was found on the potential energy surface. However, we cannot rule out the possibility that the adsorption state of CO_2 described in the previous paragraph corresponds to the aforementioned local minimum, and that a transition state exists between this minimum and the dissociated state. Attempts to localize such a transition state have been made without success. In order to evaluate if the nondissociated species is a local minimum on the PES (potential energy surface), harmonic vibrational frequencies were calculated. These are gathered in Table 3. Note that none of the normal modes that involve CO_2 have an

Fig. 2 Structures of the CO_2 species adsorbed onto the clusters. The signed values correspond to the Mulliken charges. **a** CO_2 onto $Zr_2O_{14}H_{20}$. Distances in pm: O···Zr, C···O, and O···H. The torsion angle between the CO_2 axis and the Zr–O–Zr one equals 25°. **b** CO_2 onto $Zr_3O_{16}H_{20}$. Distances in pm: O···Zr and C···O. **c** CO_2 onto $Zr_3O_{19}H_{26}$. Distances in pm: O···H (*dotted lines*) and C···O (*dashed lines*). **d**) CO_2 onto $Zr_4O_{16}H_{16}$. Dissociative adsorption. **e** CO_2 onto $Zr_5O_{24}H_{28}$. Apical adsorption

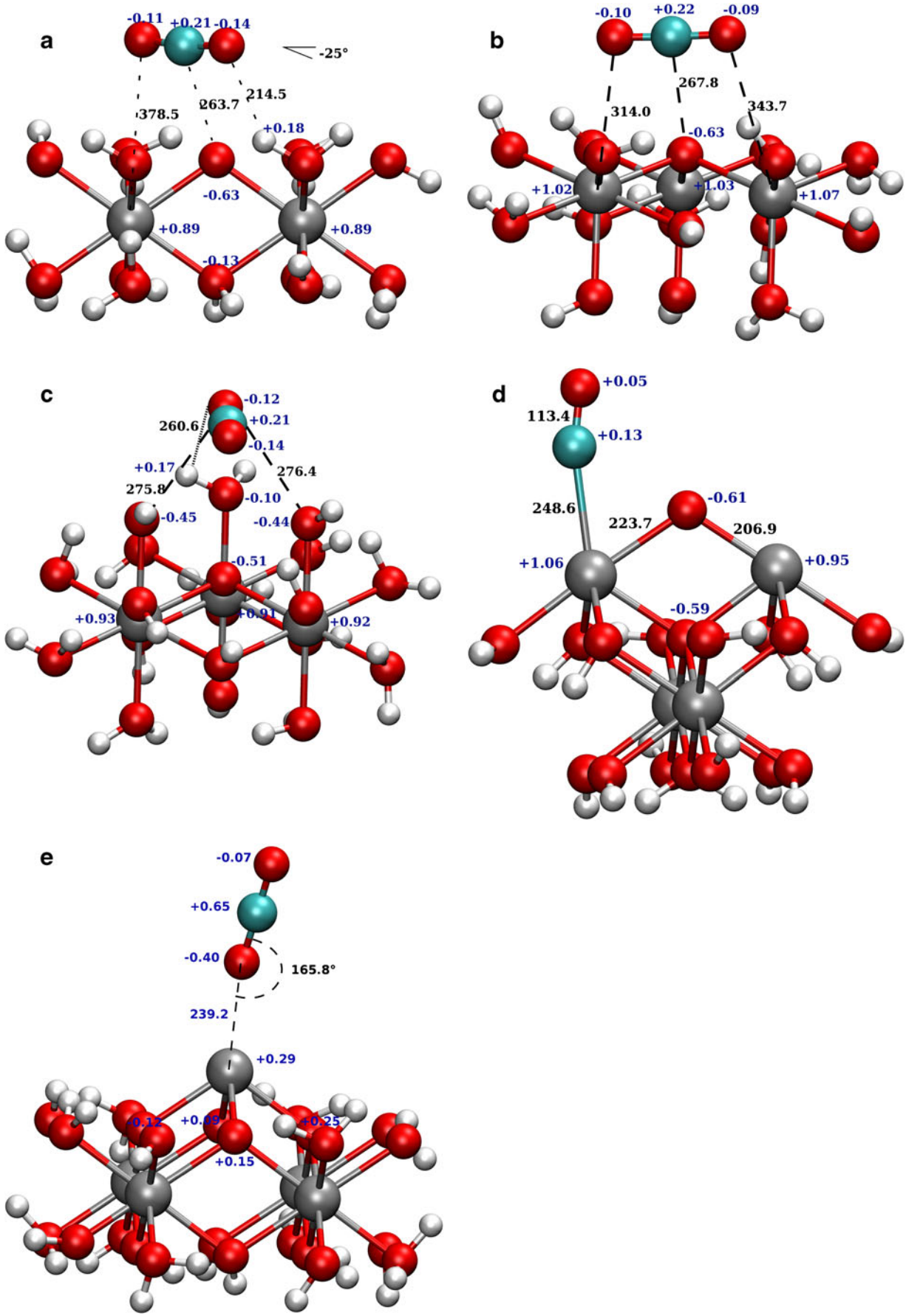
a
-0.11
+0.21
-0.14
-25°
378.5
263.7
214.5
+0.18
-0.63
+0.89
+0.89
-0.13
b
-0.10
+0.22
-0.09
267.8
314.0
343.7
-0.63
+1.02
+1.03
+1.07
c
-0.12
260.6
+0.21
-0.14
+0.17
276.4
275.8
-0.10
-0.45
-0.44
-0.51
+0.93
+0.91
+0.92
d
+0.05
113.4
+0.13
248.6
-0.61
223.7
206.9
+1.06
+0.95
-0.59
e
-0.07
+0.65
-0.40
165.8°
239.2
+0.29
+0.15

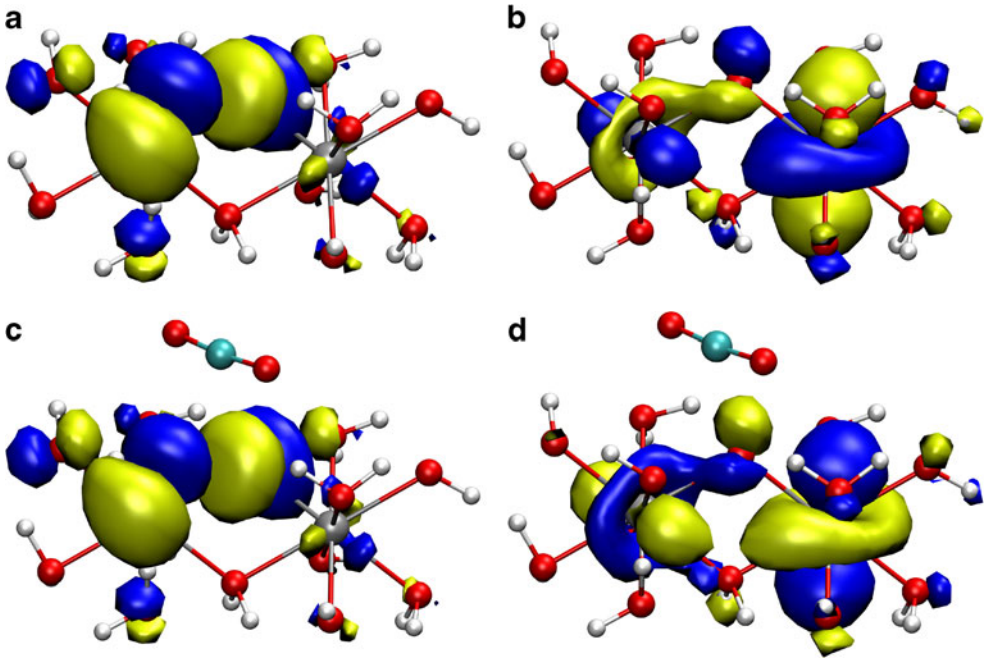

Fig. 3 Frontier orbitals of the cluster $Zr_2O_{14}H_{20}$: **a** HOMO, **b** LUMO, **c** HOMO with CO_2 adsorbed, **d** LUMO with CO_2 adsorbed

imaginary frequency, which proves that this adsorbed species is a local minimum. It is worth mentioning that if the physisorbed and chemisorbed structures are linked by a reaction pathway, the corresponding PES, or equivalently the chemical reaction coordinate, should be quite complex. In effect, the adsorbed molecule should first perform a 180° rotation for the oxygen atoms to point toward the surface, and then a translation on the surface to undergo dissociation. Most likely, the reaction coordinate is a combination of rotational and translational moves along the path. It could be that calculations based on constrained ab initio molecular dynamics would be more appropriate for carrying out this search for a transition state. However, that is beyond the scope of this work. Based on all of these results, it appears that this adsorption site is rather unstable due to the large dipole moment generated by the "missing" surface oxygen atom, so the dissociative adsorption of CO_2 leads to the reconstruction of the (001) surface (Figs. 1d and 2d). After the relaxation of the structure, the bridging atom

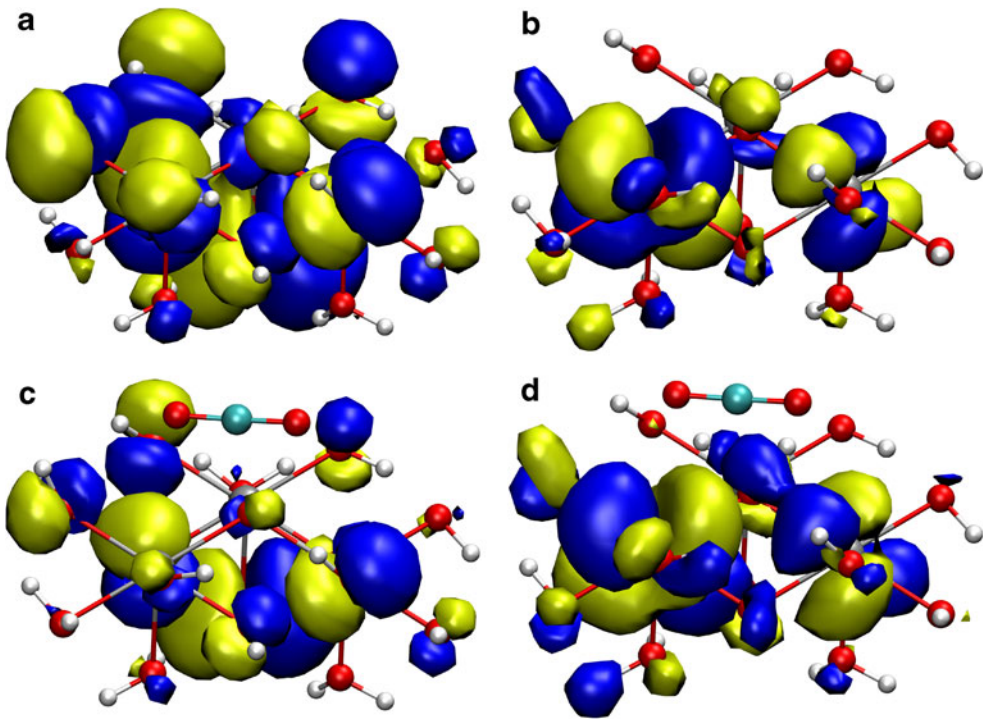

Fig. 4 Frontier orbitals of the cluster $Zr_3O_{16}H_{20}$: **a** HOMO, **b** LUMO, **c** HOMO with CO_2 adsorbed, **d** LUMO with CO_2 adsorbed

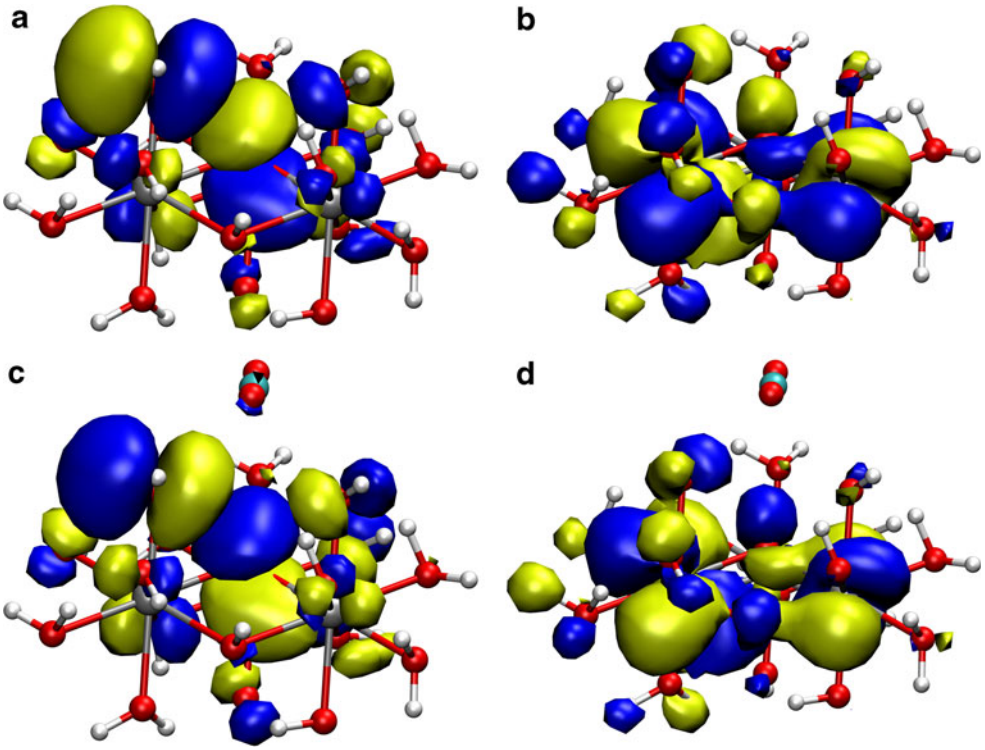

Fig. 5 Frontier orbitals of the cluster $Zr_3O_{19}H_{26}$: **a** HOMO, **b** LUMO, **c** HOMO with CO_2 adsorbed, **d** LUMO with CO_2 adsorbed

is located roughly at the crystallographic site of the oxygen atom in the bulk solid. In addition, the charge on this atom corresponds to that in the solid (Fig. 2d). The charge on the zirconium atom, which is not really affected by the presence of the adsorbate (CO), amounts to about +1 |*e*|. The carbon monoxide molecule adsorbed onto Zr is located at around 250 pm. It is then physisorbed onto the surface and interacts with the surface (probably weakly; the corresponding energy has not been calculated). This assumption is confirmed by the C–O bond distance of the adsorbed species, which is close to that of the free molecule (113.4 pm vs. 112.8 pm, respectively), as obtained from microwave spectroscopy [42]. The HOMO and LUMO of the naked cluster (Fig. 6a and b) present a very large isosurface above each zirconium atom; this corresponds to a bonding combination of the d_{yz} orbitals of Zr atoms. As CO_2 adsorbs dissociatively, the HOMO and LUMO essentially relocalize on the oxygen atoms of the cluster (π and π* orbitals, Fig. 6c and d). The chemisorption energy, which comprises both the dissociation energy of CO_2 and the relaxation on the surface, is then highly exothermic (−282.4 kJ mol^{-1}).

Table 3 Harmonic frequencies (cm^{-1}), intensities (km mol^{-1}), and vibrational motion of CO_2 adsorbed onto the cluster $Zr_4O_{16}H_{16}$

Harmonic frequency	Intensity	Vibrational motion
109.9	6.4	CO_2 wagging
133.3	6.3	CO_2 twisting
195.4	5.1	CO_2 twisting
246.9	3.8	C out-of-plane
249.0	11.9	C out-of-plane
365.3	109.8	CO_2 rocking
392.9	52.9	Symmetric ZrC stretching
722.1	64.7	CO_2 bending
1243.8	147.0	Symmetric CO + ZrC stretching
1466.0	134.2	Antisymmetric CO + ZrC stretching

$Zr_5O_{24}H_{28}$ presents a single, unsaturated, available zirconium atom on the surface (Fig. 1e). As shown in Fig. 2e, the CO_2 molecule is adsorbed in an apical position via one of the oxygen atoms. The situation where the CO_2 molecule is adsorbed by the carbon atom is not stable and spontaneously leads to the apical conformation. The adsorption energy amounts to about −65 kJ mol^{-1} and the distance between both species is 239 pm. The charge on the zirconium atom is substantially modified by the interaction with the CO_2 molecule when compared with the naked cluster. It decreases from +77 |*e*| down to +0.29 |*e*|, which corresponds to a donation of about 0.5 |*e*| from the π orbitals of CO_2 to the Zr *d* orbitals. This effect can easily be observed in the charges of the topmost C and O atoms. In addition, some of the oxygen atoms located beneath the surface also contribute drastically to the donation, as evidenced by their positive Mulliken charges (+0.09 |*e*|, +0.15 |*e*|, and +0.25 |*e*|, Fig. 2d) compared with their situation in the naked cluster (+0.07 |*e*|, −0.3 |*e*|, and −0.07 |*e*|, Fig. 1d). The strong charge transfer is particularly visible for the oxygen of CO_2 that binds with the zirconium atom: it bears a charge (−0.4 |*e*|) that is twice as large as that in the free molecule. The HOMO of $Zr_5O_{24}H_{28}$ is of binding character between the

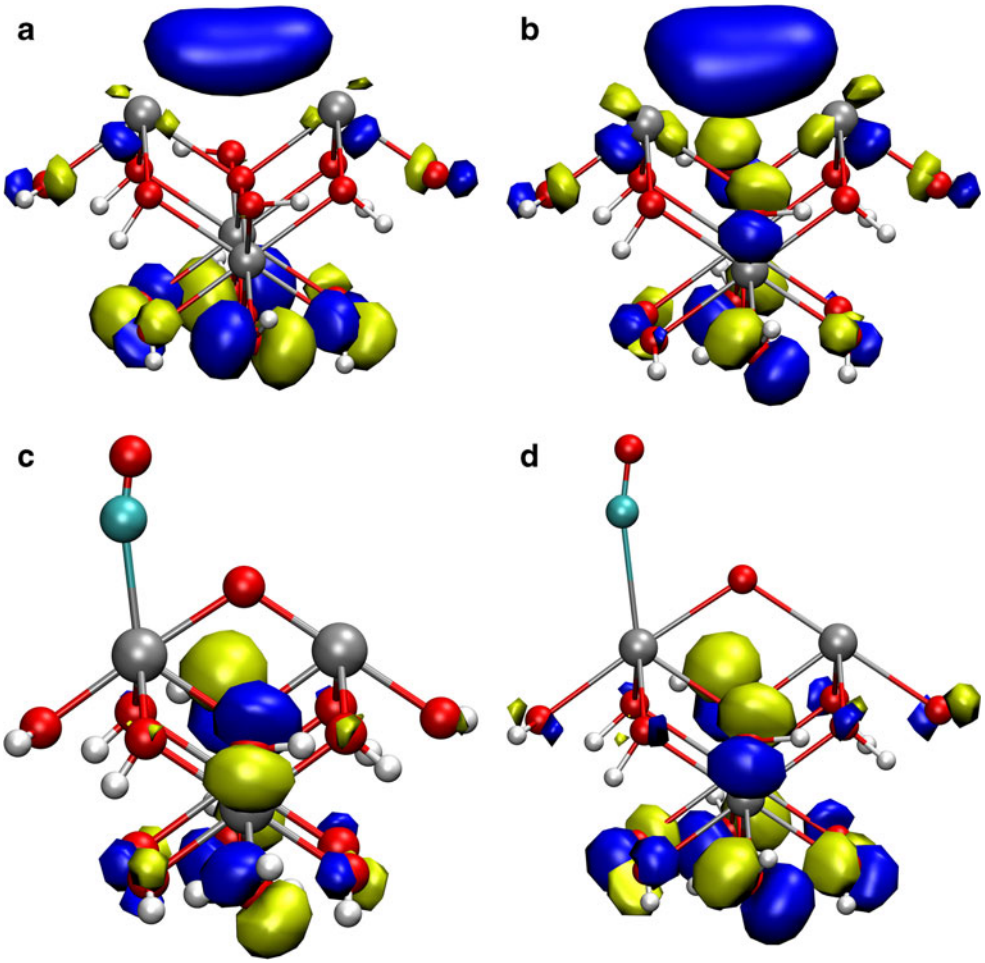

Fig. 6 Frontier orbitals of the cluster $Zr_4O_{16}H_{16}$: **a** HOMO, **b** LUMO, **c** HOMO with CO_2 adsorbed, **d** LUMO with CO_2 adsorbed

d_{xy} orbital of Zr and the *p* orbitals of the surface oxygen atoms, and is barely perturbed when CO_2 is adsorbed (Fig. 7a and c). The LUMO of the cluster consists almost totally of the d_{z2} orbital of Zr (Fig. 7b). When adsorption of CO_2 occurs, the HOMO becomes a combination of the d_{z2} orbital of Zr and the π* orbital of CO_2 (Fig. 7d).

Comparison with other systems and discussion

In this section we compare the adsorption of CO_2 onto ZrO_2 with experimental or theoretical studies of its adsorption onto other types of surfaces.

It appears that the adsorption of CO_2 onto ZrO_2 has been studied to a lesser degree than its adsorption onto other supports, be they metallic or metal oxides. Indeed, to our knowledge, there is no such report at the DFT level. In 1996, Freund and Robert published a review on the adsorption of CO_2 onto various supports [43]: (a) physisorption on Mg, Au, Ag, Bi, Ir, BaO, CaO, Cr_2O_3, MnO, NiO, TiO_2, and ZnO; (b) chemisorption on Mg, Bi, and ZnO; and (c) dissociative chemisorption on Mg, Al, Mo, and Bi. For the metals Fe, Ni, Rh, Pd, and Pt, the species of CO_2 adsorbed depends strongly on the crystallographic face and the elaboration process (film, powder, etc.). Among the transition metal oxides, only ZnO is able to yield the $CO_2^{\delta-}$ adsorbed species of CO_2. The carbonate form is obtained on the other oxides. The physisorbed and chemisorbed species that give $CO_2^{\delta-}$ are sketched in Fig. 8. According to these authors, the physisorption of CO_2 occurs at temperatures as low as 80 K. However, chemisorption leading to either the $CO_2^{\delta-}$ species or the dissociation of the molecule occurs only in very specific cases, such as on rough surfaces, when a high density of defects is present, or when surfaces are modified by the presence of alkaline atoms. This behavior was also observed in our calculations in the case where CO_2 is adsorbed onto ZrO_2 sites with defects (clusters $Zr_4O_{16}H_{16}$ and $Zr_5O_{24}H_{28}$).

In 1998, Bachiller-Baeza et al. studied the adsorption of CO_2 onto various polymorphs of ZrO_2: monoclinic, tetragonal, and/or cubic as well as monoclinic and tetragonal ones [44]. X-ray diffraction, infrared spectrometric, and microcalorimetric measurements were carried out. The X-ray diffractograms showed that the cubic and tetragonal structures of ZrO_2 are barely distinguishable due to the very similar environments of the zirconium and oxygen atoms in both structures. As a consequence, the authors did not exclude the possibility that the

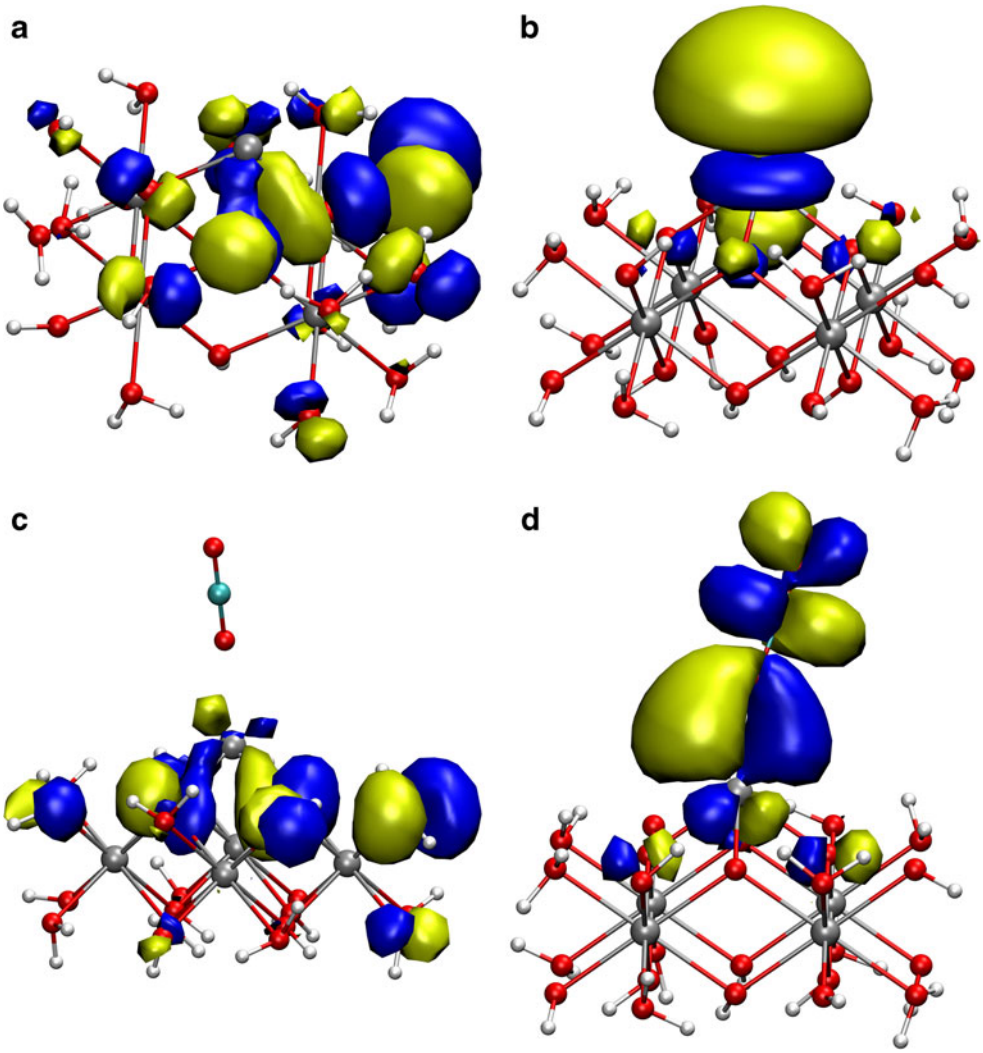

Fig. 7 Frontier orbitals of the cluster $Zr_5O_{24}H_{28}$: **a** HOMO, **b** LUMO, **c** HOMO with CO_2 adsorbed, **d** LUMO with CO_2 adsorbed

"purely" cubic or tetragonal ZrO_2 samples were in fact mixtures of both polymorphs. The cubic form is characterized by a weak concentration of hydroxyl end-groups. The OH groups are either bridged or capped species. Since the authors did not observe the formation of hydrogenocarbonate forms of CO_2 on the tetragonal (or cubic) ZrO_2, they concluded that the formation of carbonate is mediated by the presence of the hydroxyl groups, which are indeed much more abundant in monoclinic ZrO_2. The most basic species on the monoclinic ZrO_2 are, according to the authors, pairs of unsaturated Zr^{4+}–O^{2-} species. CO_2 is thus more strongly adsorbed as a bidentate carbonate than on cubic ZrO_2. Microcalorimetric measurements showed that stronger adsorption of carbon dioxide occurs on the monoclinic polymorph of ZrO_2 than on the tetragonal/cubic one.

Our results seem to agree with these experimental findings, in the sense that physisorption is the most common form of CO_2 adsorption onto cubic ZrO_2. The molecule is then only weakly perturbed (or is even unperturbed) with respect to the free one. In addition, in spite of the greater abundance of OH groups in our models of cubic zirconia than inferred from experiments, we did not observe the formation of carbonate species. It is likely, then, that the formation of carbonate species is an activated process.

Some studies have reported the adsorption of CO_2 onto transition metals (Fe, Ni, Pt) [45] and other oxide surfaces, such as TiO_2 [46–48], SnO_2 [49], ZnO [50, 51], and the alkaline earth oxides CaO, SrO, and BaO [52].

On TiO_2 [45, 46], the monodentate adsorption of CO_2 onto the surface (Fig. 8a) occurs at the acidic site (Ti) via the oxygen atom (the basic site on the molecule). The interaction distance is 223.6 pm, and the molecule is asymmetrical and highly polarized. This situation seems to be generally very similar to that observed for ZrO_2 in our calculations for $Zr_5O_{24}H_{28}$. The adsorption distance is large—even greater than that determined for TiO_2—and the molecule is polarized (see Fig. 2e). The CO bond lengths are 118.1 pm and 115.5 pm, respectively; the longest one is closest to the surface. It is noticeable that, according to the authors, there is no charge transfer between TiO_2 and CO_2: a situation which differs from that seen for the

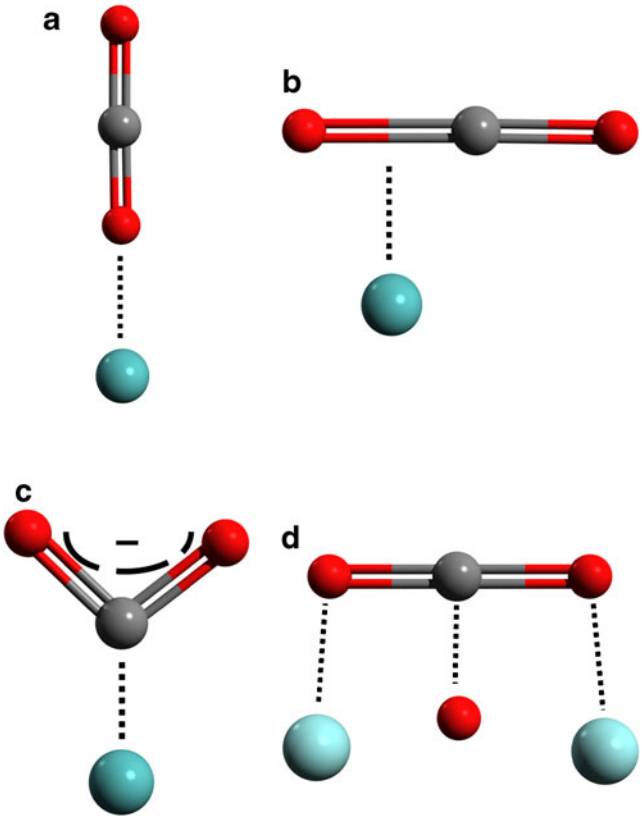

Fig. 8 Sketch of the modes of adsorption of CO_2 onto various surfaces: **a** monodentate physisorption, **b** M-ηCO_2 physisorption, **c** chemisorption of the $CO_2^{\delta-}$ species, **d** bidentate physisorption

ZrO_2/CO_2 duo. As mentioned above, the charge on Zr is greatly modified by the adsorption of CO_2, and the molecular orbitals of both species combine. There is a net gain in electron density on the oxygen near the zirconium (+0.206 $|e|$ = +0.178σ + 0.028π), a loss of electron density on the second one (−0.127 $|e|$ = +0.029σ – 0.156π), and a loss on the central atom (−0.250 $|e|$ = −0.216σ – 0.034π). Table 4 presents the calculated atomic orbital populations (OAPs) of the atoms involved in the adsorption onto $Zr_5O_{24}H_{28}$. We can see that the OAPs of the oxygen and carbon atoms are considerably modified between the free state of the molecule and the adsorbed state. Finally, in contrast with ZrO_2, the monodentate adsorption of CO_2 onto TiO_2 is the most energetic, and amounts to −79.5 kJ mol^{-1}.

The adsorption of CO_2 parallel to the surface of TiO_2 occurs preferentially with the oxygens of CO_2 pointing towards the acidic sites (Ti; see Fig. 8d) at a distance of about 237 pm (308.5 pm on average for ZrO_2). For TiO_2, the corresponding adsorption energy is close to the one found for the apical adsorption of CO_2 onto ZrO_2, namely −68.4 kJ mol^{-1}. As a consequence, the parallel adsorption of CO_2 onto TiO_2 appears to be geometrically and energetically very different from that observed for ZrO_2. However, some recent Hartree–Fock calculations using clusters ($Ti_7O_{22}H_{16}$) [48] are, in terms of energetics, in better agreement with those obtained for ZrO_2. The adsorption energy is −39.5 kJ mol^{-1}, which is much lower than that for monodentate adsorption.

Carbon dioxide is adsorbed preferentially in the monodentate state (−34.7 kJ mol^{-1}) onto the surface of tin dioxide [49], whereas the bidentate state is less favorable by about 15 kJ mol^{-1} (−19.3 kJ mol^{-1}). The sequence is then the same as for ZrO_2. However, the adsorption energy for the monodentate state is much weaker on tin oxide, showing that tin is less acidic. The adsorption distance Sn–O (233.4 pm) is similar to that found for ZrO_2 [d(Zr–O)=239.2 pm]. In bidentate adsorption, the molecule is slightly more curved (174°) on the SnO_2 surface than on the ZrO_2 one (177°). Adsorption onto the basic sites of the SnO_2 surface leads to the carbonate species CO_3^- with an adsorption energy of either −25.1 kJ mol^{-1} or −34.7 kJ mol^{-1}, depending on the orientation of the molecule with respect to the surface.

A theoretical study of the adsorption of CO_2 onto ZnO(10-10) using the ONIOM model has been reported by Lopes Martins et al. [50]. These authors used a model

Table 4 Atomic orbital populations of the atoms involved in the monodentate adsorption of CO_2 onto $Zr_5O_{24}H_{28}$

Atoms	Atomic orbital population								
	s	p_x	p_y	p_z	d_{xy}	d_{xz}	d_{yz}	d_{x2-y2}	d_{z2}
Zr	8.80	6.09	6.09	6.09	2.29	2.46	2.49	2.52	2.35
$Zr_{w\ CO2}$	8.98	6.19	6.17	6.19	2.34	2.41	2.46	2.47	2.44
O_{free}	3.92	1.49	1.51	1.25	0	0.01	0.01	0	0.01
O_{ads}	3.97	1.38	1.53	1.5	0.01	0.01	0	0.01	0
O_{ext}	3.91	1.29	1.41	1.43	0.01	0	0.01	0.01	0
C_{free}	2.97	0.81	0.82	0.73	0.01	0.07	0.09	0.01	0.05
C_{ads}	2.8	0.74	0.78	0.77	0.04	0.05	0.02	0.07	0.04

Zr metal atom in the cluster; $Zr_{w\ CO2}$ metal atom with CO_2 adsorbed onto the cluster; O_{free} oxygen atom in CO_2 in the gas phase; O_{ads} oxygen atom that interacts with the cluster during CO_2 adsorption; O_{ext} oxygen atom that does not interact with the cluster during CO_2 adsorption; C_{free} carbon atom in CO_2 in the gas phase; C_{ads} carbon atom in adsorbed CO_2

cluster containing 348 units of ZnO and three levels of approximations: molecular mechanics with the universal force field (UFF), the HF/6-21 G* method, and CCSD/6-31 + G**. Only adsorption onto the metallic center was envisaged in the study. The results show that CO_2 is adsorbed as a monodentate species, forming an angle of 23° with respect to the normal of the surface. The adsorption energy is lower than for ZrO_2 (−51.7 kJ mol^{-1}), and the metal–adsorbate distance is shorter (209.7 pm). However, according to the theoretical and experimental study of Kotsis et al. [51], CO_2 is most commonly adsorbed onto ZnO as the carbonate form.

Finally, CO_2 is adsorbed onto alkaline earth oxides as a carbonate species [52]. The absolute value of the adsorption energy increases from 125 kJ mol^{-1} up to 209 kJ mol^{-1} with the basicity of the surface (CaO < SrO < BaO). The O–C–O angle gradually decreases toward 120°, which corresponds to the bond angle in CO_3^-.

Conclusions

The adsorption of CO_2 onto clusters of zirconia has been presented. The results show that adsorption onto two adjacent zirconium atoms leads to either the dissociation or the adsorption of the molecule, depending on the geometry of the initial structure. The energy released by the process is high in either case. Adsorption onto hydroxyl groups corresponds to weak physisorption, and the molecule does not change geometrically. The adsorption of CO_2 as a monodentate species onto a single unsaturated zirconium atom yields an intermediate adsorption energy and a highly polarized molecule. Unlike other types of surfaces (e.g., SnO_2 or BaO), the carbonate species CO_3^- has not been observed to form spontaneously, which leads us to assume that the formation of this adsorbate is an activated process.

Acknowledgments The author P. Boulet is grateful to the Centre Informatique National de l'Enseignement Supérieur (CINES, Montpellier, France) and the Centre Régional de Compétences en Modélisation Moléculaire (CRCMM, Marseille, France) for providing access to their computer facilities. This work was granted access to the HPC resources of CINES under the allocation 2011085120 made by GENCI (Grand Equipement National de Calcul Intensif).

References

1. Tanabe K (1985) Surface and catalytic properties of ZrO_2. Mater Chem Phys 13:347–364
2. Sohn YH, Biederman RR, Sisson RD Jr (1994) Microstructural development in physical vapour-deposited partially stabilized zirconia thermal barrier coatings. Thin Solid Films 250:1–7
3. He MY, Ekerdt JC (1984) Methanol formation on zirconium dioxide. J Catal 90:17–23
4. Yamaguchi T, Hightower JW (1977) Hydrogenation of 1,3-butadiene with 1,3-cyclohexadiene and molecular deuterium over zirconium dioxide catalysts. J Am Chem Soc 99:4201–4203
5. Nakano Y, Iizuka T, Hattori H, Tanabe K (1979) Surface properties of zirconium oxide and its catalytic activity for isomerization of 1-butene. J Catal 57:1–10
6. Davis BH, Ganesan P (1979) Catalytic conversion of alcohols. 11. Influence of preparation and pretreatment on the selectivity of zirconia. Ind Eng Chem Prod Res Dev 18:191–198
7. Wan KT, Khouw CB, Davis ME (1996) Studies on the catalytic activity of zirconia promoted with sulfate, iron, and manganese. J Catal 158:311–326
8. Audry F, Hoggan PE, Saussey J, Lavalley JC, Lauron-Pernot H, Le Govic AM (1997) Infrared study and quantum calculations of the conversion of methylbutynol into hydroxymethylbutanone on zirconia. J Catal 168:471–481
9. Trovarelli A, Zamar F, Llorca J, de Leitenburg C, Dolcetti G, Kiss JT (1997) Nanophase fluorite-structured CeO_2-ZrO_2 catalysts prepared by high-energy mechanical milling. J Catal 169:490–502
10. Stichert W, Schuth F (1998) Synthesis of catalytically active high surface area monoclinic sulfated zirconia. J Catal 174:242–245
11. Tret'yakov NE, Pozdnyakov DV, Oranskaya OM, Filimonov VN (1970) Adsorption of some molecules on zirconium dioxide studied by an infrared spectroscopic method. Russ J Phys Chem 44:596–600
12. He MY, Ekerdt JG (1984) Infrared studies of the adsorption of synthesis gas on zirconium dioxide. J Catal 87:381–388
13. Kondo J, Abe H, Sakata Y, Maruya K, Domen K, Onishi T (1988) Infrared studies of adsorbed species of H_2, CO and CO_2 over ZrO_2. J Chem Soc Faraday Trans 84:511–519
14. Hertl W (1989) Surface chemistry of zirconia polymorphs. Langmuir 5:96–100
15. Morterra C, Orio L (1990) Surface characterization of zirconium oxide. II. The interaction with carbon dioxide at ambient temperature. Mater Chem Phys 24:247–268
16. Cerrato G, Bordiga S, Barbera S, Morterra C (1997) A surface study of monoclinic zirconia (m-ZrO_2). Surf Sci 377:50–55
17. Aboulayt A, Maugé F, Hoggan PE, Lavalley JC (1996) Combined FTIR, reactivity and quantum chemistry investigation of COS hydrolysis at metal oxide surfaces used to compare hydroxyl group basicity. Catal Lett 39:213–218
18. Tao J, Perdew JP, Staroverov VN, Scuseria GE (2003) Climbing the density functional ladder: nonempirical meta-generalized gradient approximation designed for molecules and solids. Phys Rev Lett 91:146401
19. Perdew JP, Kurth S, Zupan A, Blaha P (1999) Accurate density functional with correct formal properties: a step beyond the generalized gradient approximation. Phys Rev Lett 82:2544–2547
20. Perdew JP, Burke K, Ernzerhof M (1996) Generalized gradient approximation made simple. Phys Rev Lett 77:3865–3868
21. Staroverov VN, Scuseria GE, Tao J, Perdew JP (2003) Comparative assessment of a new nonempirical density functional: molecules and hydrogen-bonded complexes. J Chem Phys 119:12129–12137
22. Zhao Y, Truhlar DG (2005) Benchmark databases for nonbonded interactions and their use to test density functional theory. J Chem Theor Comput 1:415–432
23. Kanai Y, Wang X, Selloni A, Car R (2006) Testing the TPSS meta-generalized-gradient-approximation exchange-correlation functional in calculations of transition states and reaction barriers. J Chem Phys 125:234104
24. Zhao Y, Truhlar DG (2006) Comparative DFT study of van der Waals complexes: rare-gas dimers, alkaline-earth dimers, zinc dimer, and zinc-rare-gas dimers. J Phys Chem A 110:5121–5129
25. Grimme S (2006) Semiempirical GGA-type density functional constructed with a long-range dispersion correction. J Comput Chem 27:1787–1799

26. Schaefer A, Horn H, Ahlrichs R (1992) Fully optimized contracted Gaussian-basis sets for atoms Li to Kr. J Chem Phys 97:2571–2578
27. Boys SF, Bernardi F (1970) Calculation of small molecular interactions by differences of separate total energies—some procedures with reduced errors. Mol Phys 19:553–566
28. Whitten JL (1973) Coulombic potential energy integrals and approximations. J Chem Phys 58:4496–4502
29. Baerends EJ, Ellis DE, Ros P (1973) Self-consistent molecular Hartree–Fock–Slater calculations. I. The computational procedure. Chem Phys 2:41–51
30. Dunlap BI, Connolly JWD, Sabin JR (1979) On some approximations in applications of Xalpha theory. J Chem Phys 71:3396–3403
31. Van Alsenoy C (1988) Ab initio calculations on large molecules: the multiplicative integral approximation. J Comput Chem 9:620–626
32. Eichkorn K, Treutler O, Öhm H, Häser M, Ahlrichs R (1995) Auxiliary basis sets to approximate Coulomb potentials. Chem Phys Lett 240:283–289
33. Eichkorn K, Weigend F, Treutler O, Ahlrichs R (1997) Auxiliary basis sets for main row atoms and transition metals and their use to approximate Coulomb potentials. Theor Chem Acc 97:119–124
34. Kendall RA, Früchtl HA (1997) The impact of the resolution of the identity approximate integral method on modern ab initio algorithm development. Theor Chem Acc 97:158–163
35. Neese F (2011) The ORCA program system. Comput Mol Sci 00:1–6
36. Teufer G (1962) The crystal structure of tetragonal ZrO_2. Acta Crystallogr 15:1187
37. Patil RN, Subbarao EC (1970) Monoclinic-tetragonal phase transition in zirconia: mechanism, pretransformation and coexistence. Acta Crystallogr A 26:535–542
38. Jing-Lin Y, Guo-Chang J, Song-Hua Y, Jin-Chang M, Kuang-Di X (2001) Temperature dependence of the Raman spectra and phase transition of zirconia. Chin Phys Lett 18:991–993
39. Sekulić A, Furić K, Stubičar M (1997) Raman study of phase transitions in pure and alloyed zirconia induced by ball-milling and a laser beam. J Mol Struct 410–411:275–279
40. Gripp J, Mader H, Dreizler H, Teffo JL (1995) The microwave spectrum of carbon dioxide ^{17}OCO and ^{18}OCO. J Mol Spectrosc 172:430–434
41. Fuentealba P, Simón-Manso Y (1999) Basis set superposition error in atomic cluster calculations. Chem Phys Lett 314:108–113
42. Gilliam OR, Johnson CM, Gordy W (1950) Microwave spectroscopy in the region from two to three millimeters. Phys Rev 78:140–144
43. Freund HJ, Roberts MW (1996) Surface chemistry of carbon dioxide. Surf Sci Rep 25:225–273
44. Bachiller-Baeza B, Rodriguez-Ramos I, Guerrero-Ruiz A (1998) Interaction of carbon dioxide with the surface of zirconia polymorphs. Langmuir 14:3556–3564
45. Wang SG, Liao XY, Cao DB, Huo CF, Li YW, Wang J, Jiao H (2007) Factors controlling the interaction of CO_2 with transition metal surfaces. J Phys Chem C 111:16934–16940
46. Markovits A, Fahmi A, Minot C (1996) A theoretical study of CO_2 adsorption on TiO_2. J Mol Struct (THEOCHEM) 371:219–235
47. Ahdjoudj J, Markovits A, Minot C (1999) Hartree–Fock periodic study of the chemisorption of small molecules on TiO_2 and MgO surfaces. Catal Today 50:541–551
48. Takahashi H, Yuki K, Nitta T (2002) Chemical modification of rutile TiO_2(110) surface by ab initio calculations for the purpose of CO_2 adsorption. Fluid Phase Equilibr 194–197:153–160
49. Melle-Franco M, Pacchioni G, Chadwick AV (2001) Cluster and periodic ab initio calculations on the adsorption of CO_2 on the SnO_2(110) surface. Surf Sci 478:25–34
50. Lopes Martins JB, Longo E, Rodríguez Salmon OD, Espinoza VAA, Taft CA (2004) The interaction of H_2, CO, CO_2, H_2O and NH_3 on ZnO surfaces: an ONIOM study. Chem Phys Lett 400:481–486
51. Kotsis K, Stodt D, Staemmler V, Kovacik R, Meyer B, Traeger F, Langenberg D, Strunskus T, Kunat M, Wöll C (2008) CO_2 adlayers on the mixed terminated ZnO(10-10) surface studied by he atom scattering, photoelectron spectroscopy and ab initio electronic structure calculations. Z Phys Chem 222:891–915
52. Schneider WF (2004) Qualitative differences in the adsorption chemistry of acidic (CO_2, SO_x) and amphiphilic (NO_x) species on the alkaline earth oxides. J Phys Chem B 108:273–282